JACS
JOURNAL OF THE AMERICAN CHEMICAL SOCIETY

Communication

pubs.acs.org/JACS

A Convenient Method for Preparing Alkyl-Functionalized Silicon Nanocubes

Zhenyu Yang,[†] Alexander R. Dobbie,[†] Kai Cui,[‡] and Jonathan G. C. Veinot*[,†,‡]

[†]Department of Chemistry, University of Alberta, Edmonton, Alberta T6G 2G2, Canada

[‡]NRC-National Institute for Nanotechnology, Edmonton, Alberta T6G 2M9, Canada

Supporting Information

ABSTRACT: The first solid-state synthesis of diamond structure silicon nanocube structures with edge lengths of 8−15 nm is reported. It is well-established that controlled high-temperature processing of hydrogen silsesquioxane produces exceptionally well-defined pseudospherical silicon nanocrystals. However, only a small number of accounts outlining shape-controlled synthesis have appeared. We report here that, upon prolonged annealing in an oxide matrix, nanocrystal surfaces thermodynamically self-optimize, yielding particles with cubic geometries. Surface functionalization of the resulting nanocubes is readily achieved via thermal hydrosilylation. Discussion will include description of the synthetic procedure, comprehensive material characterization, and the factors that lead to the formation of cubic structures.

Nanostructured silicon has received considerable attention. Much of this research focus has arisen because of its biocompatibility and suitable optical properties for various light-emitting applications.[1−4] It is already established for II−VI and III−V semiconductor nanocrystals that particle-shape tailoring leads to exquisite control of material optical and chemical properties.[5,6] Beyond tailoring the characteristics of individual nanocrystals and promoting better understanding of the influence of surface chemistry (e.g., surface reconstruction) on silicon nanocrystals (Si-NC) properties, nanocrystal morphology also plays an important role in their assembly into larger extended structures. Nanocrystal superstructures have received much attention because of their tunable particle components. The properties of these extended structures show great promise for the use of these structures as active systems in many devices.[7] Most superlattice structures are made up of pseudospherical particles; still, there are benefits offered by achieving other particle shapes.[8,9] For example, nanocubes offer more efficient space filling compared to their pseudospherical counterparts.

Colloidal synthesis offers a convenient method for tailoring the shapes of II−VI and III−V NCs as well as metal and metal oxide nanoparticles. This is made possible by altering/controlling the position of thermodynamic dissolution/crystallization equilibria. Preferential growth of given crystal faces can be achieved through the addition of reagents (e.g., surfactants) that selectively bond to crystal faces, thereby altering their relative thermodynamic stability. Similar solution approaches are not readily applied to Group 14 semiconductors (e.g., Si) because of their limited compatibility with solution syntheses. Unfortunately, because of the complex chemistry of silicon and its strong directional bonding, shape-controlled Si-NC synthesis is nontrivial—few examples exist.

The majority of Si- and Ge-NCs, regardless of the synthetic method employed, are spherical or pseudospherical.[10−12] It is possible to use solvothermal techniques and controlled colloidal synthesis to form cube-shaped Ge nanocrystals, but particle dimensions are large (i.e., >80 nm).[13] Silicon tetrahedra with edge dimensions larger than 100 nm have also been synthesized using solution-based methods.[14,15] In all of these cases the NCs are very large—this observation is consistent with directed NC growth rather than equilibrium-driven processes implicated in the colloidal phase-shape evolution of II−VI and III−V materials (*vide supra*). Nonthermal plasma processing of silane is an attractive alternative method for shape-controlled Si-NC synthesis that produces nanocubes with edge dimensions of approximately 35 nm.[16] Unfortunately, these relatively large nanocrystals are not readily compatible with solution processing and lie outside the size regime where quantum confinement is observed. In this regard, a new straightforward method for preparing small, solution-compatible, crystalline Si nanocubes is appealing.

In 2006, we reported well-defined, oxide-embedded spherical Si nanoparticles could be synthesized via high-temperature processing of hydrogen silsesquioxane (HSQ).[17] These Si-NCs were readily liberated via aqueous HF etching and their surfaces tailored via thermal and photochemical hydrosilylation. The size and crystallinity of these nanoparticles could be tailored by defining the processing temperature.[18] Generally, nanoparticles prepared at 1100 °C were crystalline, and high-temperature (i.e., > 1400 °C) annealing led to increased size polydispersity and faceted structures. These observations were consistent with Ostwald ripening arising from increased silicon atom diffusion associated with softening of the oxide matrix (i.e., the solid oxide matrix behaves like a viscous solvent).[19] To date, direct evaluation of the influence of annealing time on NC morphology has largely been overlooked for oxide-embedded Si-NCs. Herein, we report that processing of an oxygen-deficient sol−gel derived precursor using a two-stage high-temperature annealing allows formation of Si nanocubes with edge lengths of ∼8−15 nm.

The general method for preparing silicon nanocubes is summarized in Scheme S1 (Please see Supporting Information

Received: June 24, 2012

   dx.doi.org/10.1021/ja3061497 | J. Am. Chem. Soc. XXXX, XXX, XXX−XXX

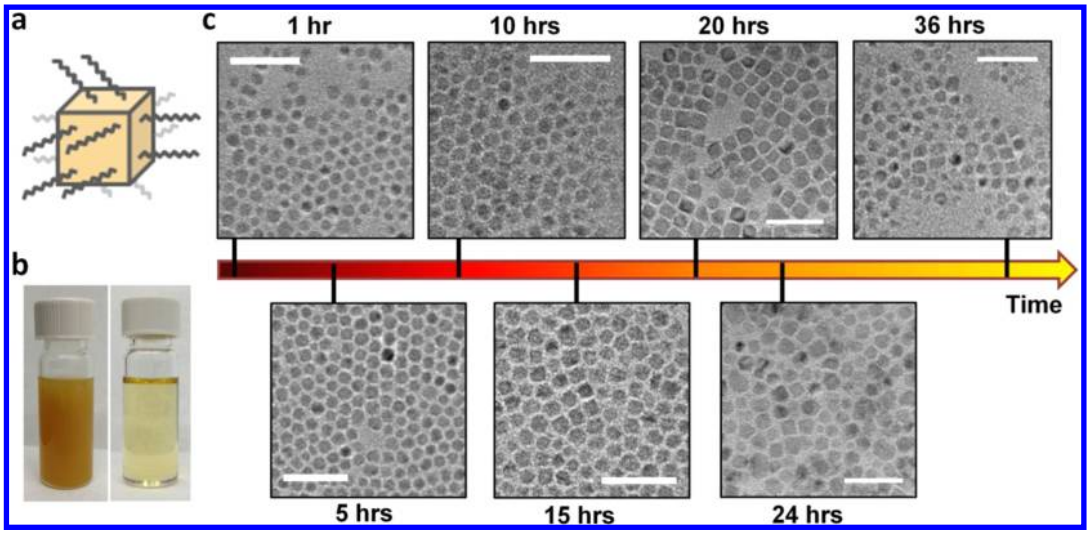

Figure 1. Dodecene-functionalized Si nanocubes. (a) Schematic of functionalized Si nanocubes. (b) Image of functionalized Si nanocubes dispersed in toluene before (left) and after (right) filtration. (c) Bright field TEM images (scale bar = 50 nm) showing the influence of annealing time on size and shape of Si-NCs and Si nanocubes formed after annealing at 1300 °C.

[SI]). HSQ was heated to 1100 °C in a slightly reducing atmosphere (5% H_2/95% Ar) to produce oxide-embedded Si-NCs. After cooling to room temperature, the resulting product was transferred to a high temperature furnace and annealed at higher temperatures (i.e., 1200, 1300, or 1400 °C) in an Ar atmosphere for predetermined times (i.e., 1−36 h). This second heating in inert atmosphere induces morphological evolution of the Si-NCs. The resulting orange/brown powder was mechanically ground and subsequently etched using a 1:1:1 HF/ethanol/water solution to liberate hydride-terminated Si-NCs and large Si pieces. The freestanding particles were in turn passivated with dodecene via thermal hydrosilylation,[20] purified by centrifugation, and redispersed in toluene. Finally, large agglomerates and unfunctionalized particles were removed from the solution using a 0.45 μm PTFE syringe filter to yield a nonopalescent yellow solution. Infrared spectroscopy indicated the surfaces of the NCs were terminated with dodecyl functionalities (Figure S1, SI). Toluene solutions of these functionalized NCs showed extremely weak orange/red PL under 441 nm irradiation (Figure S2, SI). It is reasonable that this PL arises from the excitation of small Si-NC impurities (~3 nm) present in solution;[20] no PL from large NCs or cubes was detected. A typical nanocube synthesis employs ~0.25 g of HSQ and yields ~3.5 mg of functionalized Si nanocubes.

Annealing temperature and time are key to Si nanocube formation. Extended annealing at 1100 and 1200 °C leads to Si-NC growth as confirmed by XRD and TEM (Figures S3 and S4, SI). Peak narrowing in XRD patterns arising from increased NC size is evident when the annealing time is extended from 1 to 24 h. Consistent with these observations, TEM imaging of liberated particles indicates Si-NCs synthesized at 1100 °C are 2.9 ± 0.5 nm after 1 h processing and 7.6 ± 1.3 nm after 24 h. A similar trend was observed for Si-NCs annealed at 1200 °C. Si-NCs obtained from etching Si/SiO_2 composites annealed for 1 h at 1200 °C exhibited an average diameter of 4.7 ± 0.9 nm; this increased to 7.1 ± 2.0 nm for composites processed for 24 h. Of important note, the general pseudospherical shape of the Si-NCs was maintained even after prolonged annealing (i.e., 24 h) at 1100 °C; however, for samples processed at 1200 °C some faceted NCs were observed (Figure S4d, SI).

As one would expect, extended heating at 1300 °C also leads to evolution of Si-NC morphology (see Figure 1). Processing for 1 h yields pseudospherical NCs with TEM evaluated diameters of 7.9 ± 1.3 nm. Initially, annealing favors pseudospherical particle growth (i.e., 5 h, d = 8.2 ± 1.3 nm; 10 h, d = 8.3 ± 1.5 nm; 15 h, d = 9.1 ± 1.6 nm) (Figure S5, SI). A small population of faceted structures is noted in TEM images of functionalized Si-NCs liberated from the sample processed for 15 h (Table S1, SI). To our surprise, 70% of the functionalized NCs obtained from samples processed for 20 h were cubic and exhibited a relatively narrow size distribution (Figure 1c). Extending the annealing time decreases the yield of cubes; after 24 h only 34% of the particles are cubes. After 36 h few cube structures remain (~7%), and the average size of particles becomes slightly smaller (Figure S5g, SI).

With this observation in hand, the question arises, why do Si nanocubes form after 20-h processing? We have already established silicon atoms readily diffuse through the oxide matrix at higher temperatures. It is also reasonable, upon prolonged annealing, that silicon atoms rearrange to form larger faceted structures in order to minimize surface energy. Simulations suggest Si nanocubes are thermodynamically favored over their pseudospherical counterparts when their surfaces are passivated.[21] In this context, under the present processing conditions, Si-NC shape is expected to evolve to minimize surface energy leading to the most stable cube geometry with the lowest energy surfaces (i.e., {111} and {110}). As the particles grow with longer annealing, preferential formation of the cube shape is lost because the oxide-embedded nanodomains coalesce and yield larger silicon pieces upon removal of the oxide with HF. These large pieces of silicon appear porous and are the subject of ongoing investigation.

Consistent with our proposal of why cubic structures form, we have found the presented approach to be quite general and it is only necessary to identify suitable parameters (e.g., time and temperature). For example, Si nanocubes may also be obtained from reactions performed at higher temperatures over shorter times (e.g., 1400 °C/1 h, not shown) presumably because of more rapid diffusion of silicon atoms. This is the subject of ongoing investigation in our laboratory.

dx.doi.org/10.1021/ja3061497 | J. Am. Chem. Soc. XXXX, XXX, XXX−XXX

We now turn our attention to a more detailed examination of the Si nanocubes obtained after 20 h of annealing at 1300 °C. Figure 2 shows electron microscopy images confirming the size and morphology of the Si nanocubes (edge length = 12.1 ± 2.7 nm) with aspect ratios of ∼1−1.5 (Figure S6, SI). Selected area electron diffraction (SAED, Figure 2e) clearly shows diffraction patterns consistent with diamond structure silicon. A comparison of the intensity ratio for diffraction rings obtained for pseudospherical ($I_{(111)}$:$I_{(220)}$ = 1.58) and cubic ($I_{(111)}$:$I_{(220)}$ = 1.70) particles is consistent with some oriented growth of the nanocrystals. Energy-dispersive X-ray spectroscopy (EDX, Figure 2b) confirms the presence of silicon and a small amount of oxygen because of the limited surface passivation by alkyl chains and air exposure during handling. To determine the "true" shape of the silicon core and eliminate any influence arising from surface ligands, the Si particles were analyzed by high-angle annular dark-field (HAADF) imaging. The HAADF image (Figure 2c) highlights Si nanocubes with edge dimensions of ∼8−15 nm showing higher *Z*-contrast indicating an enriched Si content.

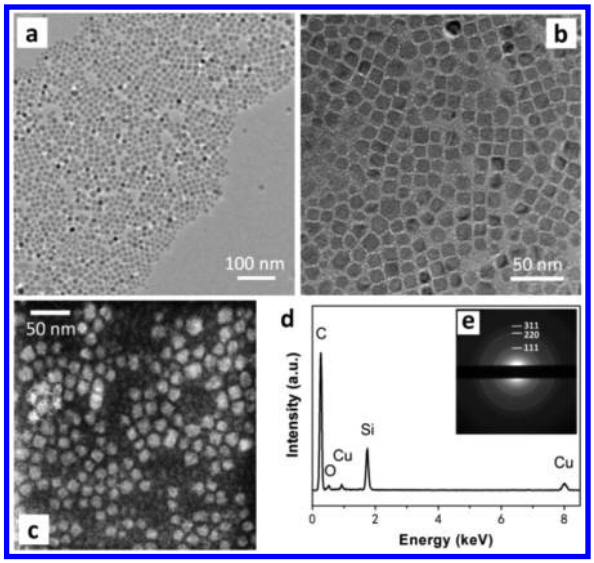

Figure 2. Size and morphology analysis of dodecene functionalized silicon nanocubes formed from 1300 °C after 20 h annealing. (a, b) Bright-field TEM and (c) HAADF images of Si-NCs. (d) EDX spectrum and (e) SAED ring patterns of Si-NCs. C and Cu signals arise from the sample grid.

High-resolution TEM (HRTEM) imaging provided valuable information regarding the crystal structure of the present Si nanocubes (Figure 3). The periphery of each Si particle is highlighted with a dashed parallelogram for clarity. The majority of the Si nanocubes examined showed lattice fringes spaced by 0.33 nm, perpendicular to [111] direction and parallel to one of the square edges. This spacing is close to that of the bulk {111} atomic plane spacing (i.e., 0.32 nm) for diamond-structured Si and consistent with that reported for other silicon nanostructures.[22−24] A small subset of the nanocubes showed two sets of lattice fringes (Figure 3b), which were assigned specifically to perpendicular [111] and [11$\bar{1}$] directions with an angle between them of ∼70°. In addition to those particles that showed lattice fringes, a small number of Si nanocubes analyzed lacked any obvious lattice fringes, the observation of which may be the result of a misalignment of the particles with the electron beam.

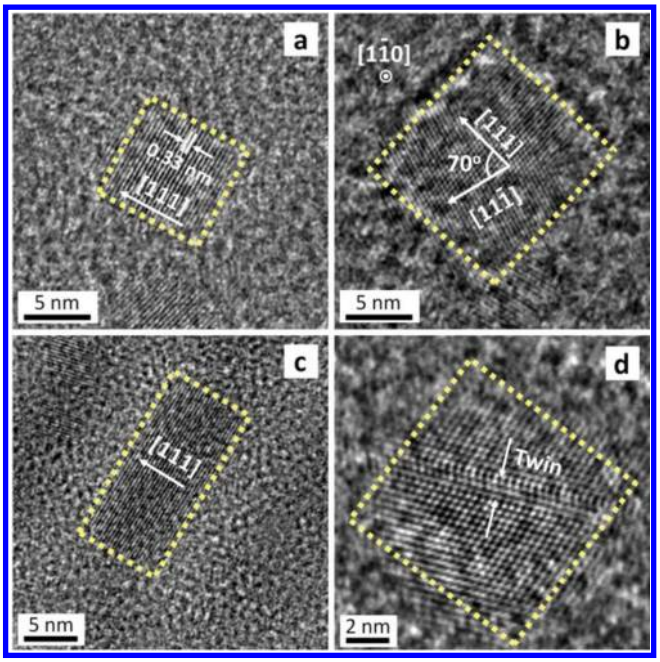

Figure 3. HRTEM images of silicon nanocubes. (a) A set of lattice fringes perpendicular to [111] direction and parallel to the cube edge. (b) Two sets of fringes perpendicular specifically to [111] and [11$\bar{1}$] directions. Projection direction parallel to [1$\bar{1}$0] is indicated. (c) A cuboid Si nanoparticle. (d) Twinned structure in one Si cube.

No extended defects (i.e., dislocations and stacking faults) were obvious in the presented analysis. We did note a small number of Si cubes displaying twinned structures (Figure 3d). Detecting these twinned structures is only possible if the twinning boundary is aligned appropriately (i.e., parallel or almost parallel) with the incident electron beam direction.[25] This orientation dependence may account for the small number of particles displaying twinning that were detected.

From the present observations we conclude that most of the Si nanocubes grow in the [111] direction, while small subpopulations grow in the [1$\bar{1}$0] and [11$\bar{2}$] directions (Figure 3c). The preferential growth direction may be understood when considering the comparatively low surface energy of the {111} and {110} silicon surfaces versus that of the {100}.[26] In this context, we propose the annealing-induced evolution of the present particles is thermodynamically driven and cubes form in response to minimization of surface energy.

Definitive conclusions regarding the exact ordering of atoms on the nanocube surfaces must be made with caution because surface reconstruction cannot be ignored. Still, it is possible to make some reasonable proposals on the basis of Figure 3. Figure 3a suggests two faces of the cubes exhibit the {111} atomic arrangement. Figure 3b suggests some may prefer {110} ordering based upon the electron beam direction. In this regard, we propose the resulting nanocubes are terminated by (1$\bar{1}$0), (111), and (11$\bar{2}$) faces. Figure S7 (in SI) illustrates how a cubic structure can be derived from a three-dimensional model of diamond lattice silicon by terminating the structure by these crystal faces. More detailed surface crystallographic studies are the subject of ongoing investigations.

In this report we have demonstrated annealing time and temperature can affect the morphology of Si-NCs formed during the disproportionation of HSQ. In doing so, we have found it is possible to exploit the relative thermodynamic stabilities of Si crystal faces to induce silicon nanocrystal shape

dx.doi.org/10.1021/ja3061497 | *J. Am. Chem. Soc.* XXXX, XXX, XXX−XXX

evolution in an oxide matrix. Such oxide-embedded Si cubes can be liberated without compromising their shape and subsequently passivated using thermochemical functionalization. Future work will trace the shape evolution of Si-NCs, investigate the atom arrangement on the surfaces of Si cubes, and further refine the annealing parameters to increase size and shape control.

■ ASSOCIATED CONTENT

Supporting Information

Experimental details and additional characterization of silicon nanocrystals and silicon nanocube structures. This material is available free of charge via the Internet at http://pubs.acs.org.

■ AUTHOR INFORMATION

Corresponding Author

jveinot@ualberta.ca

Notes

The authors declare no competing financial interest.

■ ACKNOWLEDGMENTS

We acknowledge funding from the Natural Sciences and Engineering Research Council of Canada (NSERC), Canada Foundation for Innovation (CFI), Alberta Science and Research Investment Program (ASRIP), and University of Alberta Department of Chemistry. C. W. Moffat, M. Sjkel and G. Popowich are thanked for assistance with FT-IR and TEM. We also thank R. A. Lockwood and Dr. A. Meldrum (Department of Physics, University of Alberta) for the assistance with PL measurement. All Veinot Team members are thanked for useful discussion.

■ REFERENCES

(1) Maltzahn, G. v.; Park, J.-H.; Lin, K. Y.; Singh, N.; Schwöppe, C.; Mesters, R.; Berdel, W. E.; Ruoslahti, E.; Sailor, M. J.; Bhatia, S. N. *Nat. Mater.* **2011**, *10*, 545−552.

(2) Erogbogbo, F.; Yong, K.-T.; Roy, I.; Xu, G. X.; Prasad, P. N.; Swihart, M. T. *ACS Nano* **2008**, *2*, 873−878.

(3) Holman, Z. C.; Liu, C.; Kortshagen, U. R. *Nano Lett.* **2010**, *10*, 2661−2666.

(4) Puzzo, D. P.; Henderson, E. J.; Helander, M. G.; Wang, Z.; Ozin, G. A.; Lu, Z. *Nano Lett.* **2011**, *11*, 1585−1590.

(5) Burda, C.; Chen, X.; Narayanan, R.; El-Sayed, M. A. *Chem. Rev.* **2005**, *105*, 1025−1102.

(6) Zhuang, Z.; Peng, Q.; Li, Y. *Chem. Soc. Rev.* **2011**, *40*, 5492−5513.

(7) Talapin, D. V.; Lee, J.; Kovalenko, M. V.; Shevchenko, E. V. *Chem. Rev.* **2010**, *110*, 389−458.

(8) Demortière, A.; Launois, P.; Goubet, N.; Albouy, P. A.; Petit, C. *J. Phys. Chem. B* **2008**, *112*, 14583−14592.

(9) Stebe, K. J.; Lewandowski, E.; Ghosh, M. *Science* **2009**, *325*, 159−160.

(10) Pettigrew, K. A.; Liu, Q.; Power, P. P.; Kauzlarich, S. M. *Chem. Mater.* **2003**, *15*, 4005−4011.

(11) Warner, J. H.; Hoshino, A.; Yamamoto, K.; Tilley, R. D. *Angew. Chem., Int. Ed.* **2005**, *44*, 4550−4554.

(12) Hessel, C. M.; Reid, D.; Panthani, M. G.; Rasch, M. R.; Goodfellow, B. W.; Wei, J.; Fujii, H.; Akhavan, V.; Korgel, B. A. *Chem. Mater.* **2012**, *24*, 393−401.

(13) Wang, W.; Huang, J.; Ren, Z. *Langmuir* **2005**, *21*, 751−754.

(14) Baldwin, R. K.; Pettigrew, K. A.; Garno, J. C.; Power, P. P.; Liu, G.; Kauzlarich, S. M. *J. Am. Chem. Soc.* **2002**, *124*, 1150−1151.

(15) Barrett, C. A.; Dickinson, C.; Ahmed, S.; Hantschel, T.; Arstila, K.; Ryan, K. M. *Nanotechnology* **2009**, *20*, 275605.

(16) Bapat, A.; Anderson, C.; Perrey, C. R.; Carter, C. B.; Campbell, S. A.; Kortshagen, U. *Plasma Phys. Controlled Fusion* **2004**, *46*, B97−B109.

(17) Hessel, C. M.; Henderson, E. J.; Veinot, J. G. C. *Chem. Mater.* **2006**, *18*, 6139−6146.

(18) Hessel, C. M.; Henderson, E. J.; Veinot, J. G. C. *J. Phys. Chem. C* **2007**, *111*, 6956−6961.

(19) Talapin, D. V.; Rogach, A. L.; Haase, M.; Weller, H. *J. Phys. Chem. B* **2001**, *105*, 12278−12285.

(20) Kelly, J. A.; Veinot, J. G. C. *ACS Nano* **2010**, *4*, 4645−4656.

(21) Hawa, T.; Zachariah, M. R. *J. Phys. Chem. C* **2008**, *112*, 14796−14800.

(22) Yang, Y.; Wu, S.; Chiu, H.; Lin, P.; Chen, Y. *J. Phys. Chem. B* **2004**, *108*, 846−852.

(23) Liu, S.; Kobayashi, M.; Sato, S.; Kimura, K. *Chem. Commun.* **2005**, 4690−4692.

(24) Kang, Z.; Tsang, C. H. A.; Zhang, Z.; Zhang, M.; Wong, N.; Zapien, J. A.; Shan, Y.; Lee, S. *J. Am. Chem. Soc.* **2007**, *129*, 5326−5327.

(25) Williams, D. B.; Carter, C. B. *Transmission Electron Microscopy*, 2nd ed.; Springer: New York, 2009.

(26) Jaccodine, R. J. *J. Electrochem. Soc. C* **1963**, *110*, 524−527.